Ann Nucl Med (2016) 30:263–271
DOI 10.1007/s12149-015-1055-6

ORIGINAL ARTICLE

Simultaneous acquisition of ^{99m}Tc- and ^{123}I-labeled radiotracers using a preclinical SPECT scanner with CZT detectors

Masato Kobayashi[1] · Ichiro Matsunari[2,3] · Kodai Nishi[4] · Asuka Mizutani[5] · Yoshiharu Miyazaki[2] · Kazuhiro Ogai[1] · Jyunko Sugama[1] · Kazuhiro Shiba[6] · Keiichi Kawai[7] · Seigo Kinuya[8]

Received: 16 October 2015 / Accepted: 23 December 2015 / Published online: 8 January 2016

Abstract

Objective Simultaneous acquisition of ^{99m}Tc and ^{123}I was evaluated using a preclinical SPECT scanner with cadmium zinc telluride (CZT)-based detectors.

Methods 10-ml cylindrical syringes contained about 37 MBq ^{99m}Tc-tetrofosmin (^{99m}Tc-TF) or 37 MBq ^{123}I-15-(*p*-iodophenyl)-3*R*,*S*-methyl pentadecanoic acid (^{123}I-BMIPP) were used to assess the relationship between these SPECT radioactive counts and radioactivity. Two 10-ml syringes contained 100 or 300 MBq ^{99m}Tc-TF and 100 MBq ^{123}I-BMIPP to assess the influence of ^{99m}Tc upscatter and ^{123}I downscatter, respectively. A rat-sized cylindrical phantom also contained both 100 or 300 MBq ^{99m}Tc-TF and 100 MBq ^{123}I-BMIPP. The two 10-ml syringes and phantom were scanned using a pinhole collimator for rats. Myocardial infarction model rats were examined using 300 MBq ^{99m}Tc-TF and 100 MBq ^{123}I-BMIPP. Two 1-ml syringes contained 105 MBq ^{99m}Tc-labeled hexamethylpropyleneamine oxime (^{99m}Tc-HMPAO) and 35 MBq ^{123}I-labeled *N*-ω-fluoropropyl-2β-carbomethoxy-3β-(4-iodophenyl) nortropane (^{123}I-FP-CIT). The two 1-ml syringes were scanned using a pinhole collimator for mice. Normal mice were examined using 105 MBq ^{99m}Tc-HMPAO and 35 MBq ^{123}I-FP-CIT.

Results The relationship between SPECT radioactive counts and radioactivity was excellent. Downscatter contamination of ^{123}I-BMIPP exhibited fewer radioactive counts for 300 MBq ^{99m}Tc-TF without scatter correction (SC) in 125–150 keV. There was no upscatter contamination of ^{99m}Tc-TF in 150–175 keV. In the rat-sized phantom, the radioactive count ratio decreased to 4.0 % for 300 MBq ^{99m}Tc-TF without SC in 125–150 keV. In the rats, myocardial images and radioactive counts of ^{99m}Tc-TF with the dual tracer were identical to those of the ^{99m}Tc-TF single injection. Downscatter contamination of ^{123}I-FP-CIT was 4.2 % without SC in 125–150 keV. In the first injection of ^{99m}Tc-HMPAO and second injection of ^{123}I-FP-CIT, brain images and radioactive counts of ^{99m}Tc-HMPAO with the dual tracer in normal mice also were the similar to those of the ^{99m}Tc-HMPAO single injection. In the first injection of ^{123}I-FP-CIT and second injection of ^{99m}Tc-HMPAO, the brain images and radioactive counts with the dual tracer were not much different from those of the ^{123}I-FP-CIT single injection.

Conclusions Dual-tracer imaging of ^{99m}Tc- and ^{123}I-labeled radiotracers is feasible in a preclinical SPECT scanner with CZT detector. When higher radioactivity of ^{99m}Tc-labeled radiotracers relative to ^{123}I-labeled

✉ Masato Kobayashi
kobayasi@mhs.mp.kanazawa-u.ac.jp

[1] Wellness Promotion Science Center, Institute of Medical, Pharmaceutical and Health Sciences, Kanazawa University, 5-11-80 Kodatsuno, Kanazawa 920-0942, Japan

[2] Clinical Research Department, The Medical and Pharmacological Research Center Foundation, Hakui, Japan

[3] Division of Nuclear Medicine, Department of Radiology, Saitama Medical University Hospital, Saitama, Japan

[4] Department of Radioisotope Medicine, Atomic Bomb Disease Institute, Nagasaki University, Nagasaki, Japan

[5] Graduate School of Medicine, Division of Health Sciences, Osaka University, Osaka, Japan

[6] Division of Tracer Kinetics, Advanced Science Research Center, Kanazawa University, Kanazawa, Japan

[7] School of Health Sciences, College of Medical, Pharmaceutical and Health Sciences, Kanazawa University, Kanazawa, Japan

[8] School of Medical Sciences, College of Medical, Pharmaceutical and Health Sciences, Kanazawa University, Kanazawa, Japan

radiotracers is applied, correction methods are not necessarily required for the quantification of ^{99m}Tc- and ^{123}I-labeled radiotracers when using a preclinical SPECT scanner with CZT detector.

Keywords Dual tracer · ^{99m}Tc · ^{123}I · Small animal SPECT scanner · Cadmium zinc telluride

Introduction

Preclinical SPECT scanners are an important tool for molecular imaging in biomedical research and the development of new medicine [1]. Several recent scanners incorporate semiconductor materials such as cadmium zinc telluride (CZT) [2–6]. The CZT-based scanners improve energy and spatial resolution, as compared with sodium iodide (NaI) scintillation detectors, which are used in conventional SPECT scanners, in not only preclinical animal imaging but also clinical imaging.

With conventional SPECT scanners, it is difficult to separate ^{99m}Tc (140 keV) and ^{123}I (159 keV) images because the emission energies of these radiotracers are close. Accurate quantification of dual-isotope imaging is also difficult because the images are affected by scatter, cross-talk, attenuation and distance-dependent collimator response. Especially, there is substantial influence on not only downscattered ^{123}I photons in the energy window of ^{99m}Tc, but also cross-talk from primary photons of each radionuclide. Attempts have already been made to discriminate downscatter contamination and cross-talk using an energy window correction method in clinical SPECT scanners with NaI scintillation detectors [6–12]. Constrained spectral factor analysis and artificial neural networks are two promising approaches to compensate for scatter, cross-talk, and high-energy septal penetration in simultaneous ^{99m}Tc and ^{123}I imaging [7, 8]. Another method, a Monte Carlo-based joint ordered-subset expectation maximization iterative reconstruction algorithm, was applied to ^{99m}Tc/^{123}I brain or cardiac SPECT imaging [6, 9–11]. However, these methods are generally complicated and require many energy windows.

In this study, simultaneous acquisition of ^{99m}Tc- and ^{123}I-labeled radiotracers was evaluated on a preclinical SPECT scanner with a CZT-based semiconductor detector. To assess each image and the quantification, we used cylindrical syringes, cylindrical phantoms and myocardial infarction model rats injected with ^{99m}Tc-labeled tetrofosmin (^{99m}Tc-TF) [13] and ^{123}I-labeled 15-(*p*-iodophenyl)-3R,S-methyl pentadecanoic acid (^{123}I-BMIPP) [14–16], and syringes and normal mice injected with ^{99m}Tc-labeled hexamethylpropyleneamine oxime (^{99m}Tc-HMPAO) and ^{123}I-labeled *N*-ω-fluoropropyl-2β-carbomethoxy-3β-(4-iodophenyl)nortropane (^{123}I-FP-CIT).

Materials and methods

Phantoms

Two kinds of phantoms for the rat study were created: 10-ml cylindrical syringes (diameter 15.8 mm) and 250-ml rat-sized cylindrical phantoms (diameter 80 mm). For evaluation of relationship between SPECT radioactive counts (1 min acquisition) and radioactivity of ^{99m}Tc and ^{123}I, 10-ml cylindrical syringes contained about 37 MBq ^{99m}Tc-TF or ^{123}I-BMIPP were prepared and then attenuated in accordance with the radioactive decay. The radioactivity was measured using dose calibrator (Capintec, Inc.)

In two experiments with the two 10-ml cylindrical syringes, one syringe contained 100 MBq ^{99m}Tc-TF (Nihon Medi-physics Co., Ltd.) and the other contained 100 MBq ^{123}I-BMIPP (Nihon Medi-physics Co., Ltd.) to evaluate equal doses of ^{99m}Tc-TF and ^{123}I-BMIPP. In another experiment, one syringe contained 300 MBq ^{99m}Tc-TF and the other contained 100 MBq ^{123}I-BMIPP to evaluate high doses of ^{99m}Tc-TF and ^{123}I-BMIPP. For the rat-sized cylindrical phantoms, we evaluated two different versions. The first contained both 100 MBq ^{99m}Tc-TF and 100 MBq ^{123}I-BMIPP and second had both 300 MBq ^{99m}Tc-TF and 100 MBq ^{123}I-BMIPP.

For the mice study, one 1-ml cylindrical syringe (diameter 4.7 mm) contained 105 MBq ^{99m}Tc-HMPAO (Nihon Medi-physics Co., Ltd.) and the other contained 35 MBq ^{123}I-FP-CIT (Nihon Medi-physics Co., Ltd.).

Animals

All animal procedures were approved by the institutional committee at the Medical and Pharmacological Research Center Foundation and were conducted in compliance with the American Heart Association requirements regarding the use of research animals. Eight male Wister rats (8–11 weeks old, 250–320 g) and 10 male normal mice (6–8 weeks old, 31–35 g) were purchased from Japan SLC Inc. and were housed for 1 week under a 12-h light/12-h dark cycle with free access to food and water. The rats were anesthetized with an intraperitoneal injection of pentobarbital (30 mg/kg) and maintained with 2 % isoflurane (Abbott Laboratories), and then intubated and ventilated using a small animal ventilator (SN-480-7 × 2T, Shinano). After left thoracotomy and exposure of the heart, a 7–0 polypropylene suture on a small curved needle was

passed through the myocardium beneath the proximal portion of the left coronary artery (LCA), and both ends of the suture were passed through a small vinyl tube to make a snare. The suture material was pulled tightly against the vinyl tube to occlude the LCA. Myocardial ischemia was confirmed by ST-segment elevation on the electrocardiogram and regional cyanosis of the myocardial surface. The LCA was occluded for 30 min, and reperfusion was obtained by release of the snare and confirmed by a myocardial blush over the area at risk.

Description of preclinical SPECT/CT camera

The performance and features of the eXplore speCZT (GE Healthcare) have been reported previously [4]. Briefly, this system has a stationary detector with interchangeable rotating collimators. The detector consists of 10 CZT-based detector panels surrounding the field of view (FOV). Each CZT detector panel consists of 32 × 32 arrays with a pixel size of 2.46 mm × 2.46 mm.

We used a 5-pinhole collimator for rat imaging because the pinhole collimators are designed for high-resolution images with small regions of interest [17, 18]. The main characteristics of the pinhole collimators are: diameter of pinhole 1 mm, FOV diameter of single-bed position 76 mm, axial FOV of single-bed position 38 mm, bore diameter 89 mm and radius of rotation/focal length 50/70 mm. The system saves each event of the acquired data in a list-mode format including its energy, and gated electrocardiogram (ECG)/respiratory motion trigger for later, specialized analysis. Performance tests with the pinhole collimator showed that the transaxial and axial system resolution with resolution correction, and sensitivity of the scanner were, respectively, 1.20/2.18 mm [full-width half maximum (FWHM)/full-width tenth maximum (FWTM)] and 1.11/2.02 mm (FWHM/FWTM), and 138.5 cpm/MBq using a ^{99m}Tc radiotracer.

SPECT/CT scan with a pinhole collimator for rats

Experiments with cylindrical syringes, cylindrical phantoms and rats were performed using the eXplore speCZT SPECT/CT scanner with a 5-pinhole collimator for rat imaging. The voxel size of the image matrix was 0.5 mm × 0.5 mm × 0.5 mm because the voxel size of the single-orbit SPECT scan was fixed to 0.5 mm, which was determined by the step size of the table motion. The energy window for SPECT acquisition was set to 50–180 keV by default.

For the syringe and phantom experiments, two 10-ml cylindrical syringes or 250-ml rat-sized cylindrical phantoms were placed on the scanner table in the center of the FOV and scanned for approximately 30 min using the pinhole collimator.

In rat experiments, the helical scan mode was used to image the myocardium of the rats. Eight rats with myocardial infarction were fasted, with water supplied ad libitum and no food, at least 4 h before the SPECT experiments. The rats were anesthetized with 1.5–2.0 % isoflurane (Abbott Laboratories) and placed in a supine position on the scanner table. Limbs were fixed using surgical tape. Stainless steel electrodes were subsequently inserted into the skin of the right and left forelimbs to monitor and record the ECG data. Before SPECT scanning, the orientation of the myocardium was determined using a laser beam and CT imaging on the scanner. For CT images, the tube voltage and current of the X-ray tube were 60 kVp and 40 mA, respectively. The rats were injected with approximately 300 MBq of ^{99m}Tc-TF via the tail vein. Rats were scanned from 5 min after the injection using imaging parameters of 25 s/view and 72 views/pinhole (total 360 view) in 1° increments. Immediately after the first scan of ^{99m}Tc-TF, the same rats were injected with 100 MBq of ^{123}I-BMIPP and scanned again using the same scanning protocols and parameters.

SPECT/CT scan with a pinhole collimator for mice

For the 1-ml cylindrical syringe and mice study, experiments were performed using a 7-pinhole collimator for mice imaging. The voxel size of the image matrix was 0.5 mm × 0.5 mm × 0.5 mm, which was determined by the step size of the table motion. The energy window for SPECT acquisition was set to 50–180 keV by default in the list mode.

The setup for the syringes and 10 normal mice was the same as that for the rat study. Before SPECT scanning, the orientation of the brain was determined using a laser beam and CT imaging on the scanner. For CT images, the tube voltage and current of the X-ray tube were 60 kVp and 40 mA, respectively. Five of the 10 mice were injected with approximately 105 MBq of ^{99m}Tc-HMPAO via the tail vein. Mice were scanned from 5 min after the injection using imaging parameters of 36 s/view and 50 views/pinhole (total 350 view) in 1.06° increments. Immediately after the first scan of ^{99m}Tc-HMPAO, the same rats were injected with approximately 35 MBq of ^{123}I-FP-CIT and scanned again using the same scanning protocols and parameters from approximately 3 h after the injection.

The other five mice were injected with approximately 35 MBq of ^{123}I-FP-CIT via the tail vein and then scanned from approximately 3 h after the injection. Immediately after the first scan of ^{123}I-FP-CIT, the same rats were injected with approximately 105 MBq of ^{99m}Tc-HMPAO and scanned again from 5 min after the injection.

Reconstruction settings

All SPECT data were reconstructed using the three-dimensional maximum-likelihood expectation maximization algorithm with 50 iterations, with distance-dependent collimator response correction (DCC) [4]. For the parameters, the energy window was set to 125–150 keV for ^{99m}Tc imaging and 150–175 keV for ^{123}I imaging using acquisition data of 50–180 keV. Attenuation correction (AC) was not applied because AC provided low uniformity in the phantom study, and radioactive counts with and without AC were not that much different in the rat myocardial [19] mice brain studies (data not shown) in this study. Post-reconstruction filtering was also not applied because the filter affects the radioactive counts in the SPECT images. The scatter correction (SC) uses the triple-energy window (TEW) method for experiments with a single tracer of ^{99m}Tc [20]. Specifically, the TEW method was applied to the experiments with 10-ml cylindrical syringes and rat-sized phantom, and rats in the experiments with a single tracer of ^{99m}Tc-TF, and we set up to 3 keV in width for the left and right scatter as sub-windows by default. In the experiments with the dual tracers, the TEW method was not available because we could not set up the sub-window. AC, SC and DCC can be selected for the reconstruction method in our scanner, but DCC is always applied to improve image resolution.

Image analysis

After reconstruction of SPECT data, radioactive counts were obtained using the AMIDE medical imaging data examiner and OsiriX (http://homepage.mac.com/rossetantoine/osirix). The voxels of interest (VOIs) were located in the center of the syringes and phantoms. The spherical VOIs were approximately 5 mm in diameter for the experiments with 1-ml syringes, and approximately 10 mm in diameter for the 10-ml syringes and 250-ml rat-sized cylindrical phantoms. We placed spherical VOIs over normal and myocardial infarction areas in the rat study and striatum and whole brain in the mice study. In experiments with the rat-sized cylindrical phantoms and 1-ml syringes for the mice study, radioactive counts of ^{99m}Tc at 125–150 keV in the dual-tracer images were divided by those of the ^{99m}Tc single-tracer images in 125–150 keV. In addition, radioactive counts of ^{123}I at 150–175 keV in the dual-tracer images were divided by those of the ^{123}I single-tracer images in 150–175 keV, respectively.

Statistical analyses

A statistical software package (JMP® version 9, SAS Institute Inc.) was used for statistical analysis. We applied a paired *t* test, and statistically significant differences were defined as $P < 0.01$.

Results

In 10-ml cylindrical syringes including 100 MBq ^{99m}Tc or 100 MBq ^{123}I, the relationship between SPECT radioactive counts and radioactivity was excellent (Fig. 1).

In two syringes containing 100 MBq of ^{99m}Tc-TF or ^{123}I-BMIPP, the peaks of the energy spectrum were at the same levels (Fig. 2a). Accumulation of ^{99m}Tc-TF images in the 125–150 keV energy window were slightly higher than that of ^{123}I-BMIPP images in the 150–175 keV energy window (Fig. 2b). Mean radioactive counts per voxel of ^{99m}Tc-TF in 125–150 keV were 7 % higher than those of ^{123}I-BMIPP in 150–175 keV (Table 1). When SC was applied, downscatter contamination of ^{123}I-BMIPP was approximately 3.5 % of the counts per voxel of ^{99m}Tc-TF in 125–150 keV, whereas in the case without SC, the downscatter contamination was approximately 13.2 % of the counts per voxel of ^{99m}Tc-TF in 125–150 keV. With and without SC, no upscatter contamination of ^{99m}Tc-TF was observed in 150–175 keV.

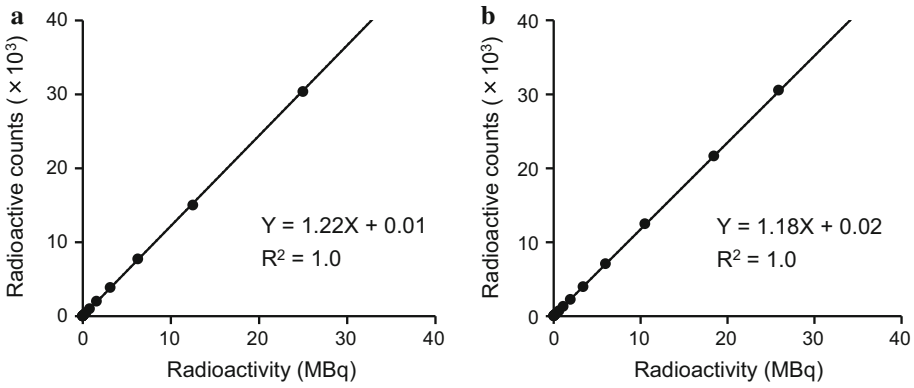

Fig. 1 The relationship between SPECT radioactive counts and 100 MBq ^{99m}Tc (**a**) and 100 MBq ^{123}I (**b**) images

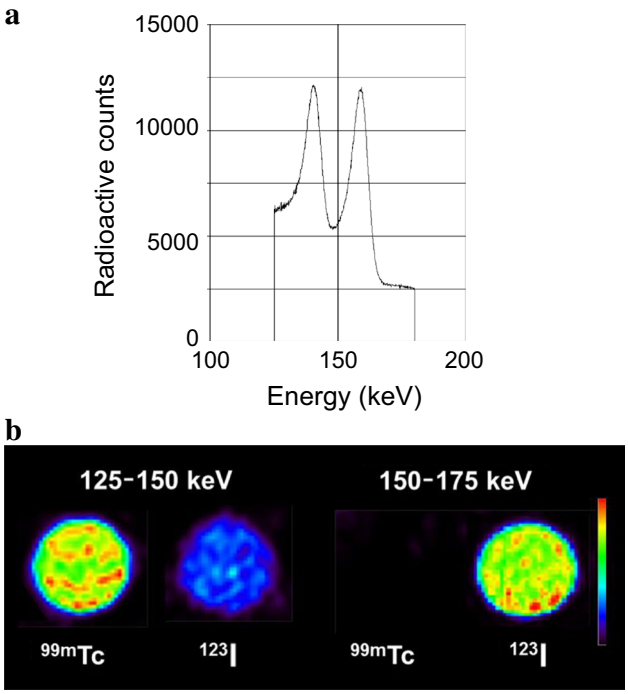

Fig. 2 Energy spectrum (**a**) and SPECT images without SC (**b**) of two cylindrical syringes with 100 MBq ^{99m}Tc-TF or 100 MBq ^{123}I-BMIPP. Energy peak of ^{99m}Tc-TF was almost the same as that of ^{123}I-BMIPP. Accumulation of ^{99m}Tc-TF images in the 125–150 keV energy window were slightly higher than that of ^{123}I-BMIPP images in the 150–175 keV energy window. Downscatter contaminations of ^{123}I-BMIPP in 125–150 keV were approximately 3.5 and 13.2 % of the radioactive counts for ^{99m}Tc-TF with and without SC, respectively. Upscatter contamination of ^{99m}Tc-TF was not observed in 150–175 keV

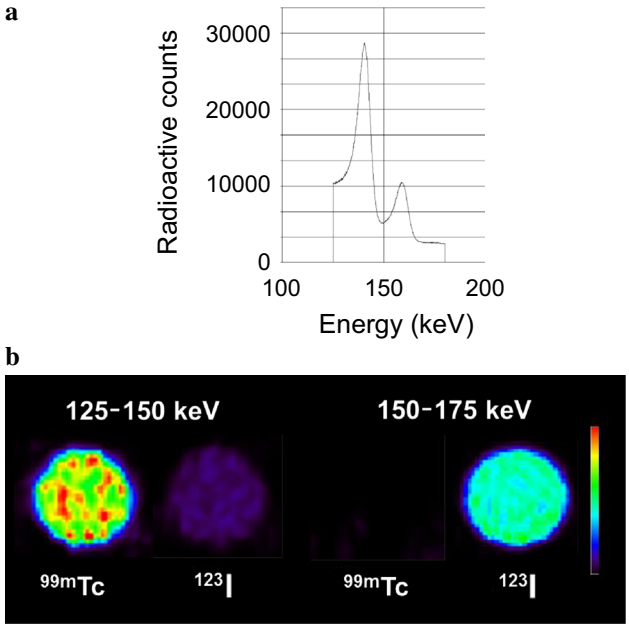

Fig. 3 Energy spectrum (**a**) and SPECT images without SC (**b**) of two cylindrical syringes with 300 MBq ^{99m}Tc-TF or 100 MBq ^{123}I-BMIPP. Energy peak of ^{99m}Tc-TF was approximately 3-fold higher than that of ^{123}I-BMIPP. ^{99m}Tc-TF image in 125–150 keV was significantly different from that of ^{123}I-BMIPP in 150–175 keV. Downscatter contaminations of ^{123}I-BMIPP in 125–150 keV were, respectively approximately 0.9 and 4.1 % of the radioactive counts for ^{99m}Tc-TF with and without SC

In two syringes including 300 MBq ^{99m}Tc-TF and 100 MBq ^{123}I-BMIPP, the peak of the energy spectrum of ^{99m}Tc-TF was almost 3-fold higher than that of ^{123}I-BMIPP (Fig. 3a). Mean radioactive counts per voxel of ^{99m}Tc-TF in 125–150 keV were also 3.3-fold higher than that of ^{123}I-BMIPP in 150–175 keV without SC (Table 2). Downscatter contaminations of ^{123}I-BMIPP were approximately 0.9 and 4.0 % of the radioactive counts for ^{99m}Tc-TF in 125–150 keV with and without SC, while there was no upscatter contamination of ^{99m}Tc-TF in 150–175 keV.

In the rat-sized cylindrical phantom including 100 MBq of ^{99m}Tc-TF and ^{123}I-BMIPP as the dual tracer (Table 3), the SC of the TEW method was not applied because we could not increase the number of energy windows in the TEW method for dual-tracer imaging. The ratios of radioactive counts of the dual tracer without SC to single tracer of ^{99m}Tc-TF in 125–150 keV became 1.21. When 300 MBq ^{99m}Tc-TF and 100 MBq ^{123}I-BMIPP were used, the ratios were 1.08. There was almost no upscatter contamination of ^{99m}Tc-TF in 150–175 keV.

In the rat model of myocardial infarction (Fig. 4), the ^{99m}Tc-TF images in 125–150 keV for the dual tracer without SC were not different from those of ^{99m}Tc-TF for the single tracer with SC. ^{123}I-BMIPP images showed no accumulation in the infarction area compared to ^{99m}Tc-TF. Mean radioactive counts of ^{99m}Tc-TF in 125–150 keV for the dual tracer were not much different from those of ^{99m}Tc-TF for the single tracer in the normal and infarction

Table 1 Radioactive counts per voxel in the 10-ml cylindrical syringes including 100 MBq ^{99m}Tc-TF and 100 MBq ^{123}I-BMIPP

	SC–				SC+			
Energy window (keV)	125–150		150–175		125–150		150–175	
Radiotracers	^{99m}Tc-TF	^{123}I-BMIPP	^{99m}Tc-TF	^{123}I-BMIPP	^{99m}Tc-TF	^{123}I-BMIPP	^{99m}Tc-TF	^{123}I-BMIPP
Counts/voxel	413.3 ± 23.2	54.4 ± 9.5	1.5 ± 0.5	382.6 ± 19.8	361.1 ± 21.2	12.6 ± 7.5	0.5 ± 0.5	335.3 ± 20.2

SC scatter correction, *^{99m}Tc-TF* ^{99m}Tc-labeled tetrofosmin, *^{123}I-BMIPP* ^{123}I-labeled 15-(*p*-iodophenyl)-3R,S-methyl pentadecanoic acid

Table 2 Radioactive counts per voxel in the 10-ml cylindrical syringes including 300 MBq ^{99m}Tc-TF and 100 MBq ^{123}I-BMIPP

	SC–				SC+			
Energy window (keV)	125–150		150–175		125–150		150–175	
Radiotracers	^{99m}Tc-TF	^{123}I-BMIPP	^{99m}Tc-TF	^{123}I-BMIPP	^{99m}Tc-TF	^{123}I-BMIPP	^{99m}Tc-TF	^{123}I-BMIPP
Counts/voxel	1294.7 ± 50.6	52.1 ± 9.1	1.3 ± 0.3	392.5 ± 21.4	1144.1 ± 53.1	10.6 ± 3.8	0.6 ± 0.5	332.5 ± 18.1

SC scatter correction, *^{99m}Tc-TF* ^{99m}Tc-labeled tetrofosmin, *^{123}I-BMIPP* ^{123}I-labeled 15-(*p*-iodophenyl)-3R,S-methyl pentadecanoic acid

Table 3 Ratios of radioactive counts in dual tracer without SC to single tracer with SC on ^{99m}Tc-TF images in 125–150 keV and ^{123}I-BMIPP images in 150–175 keV in the rat-sized cylindrical phantom

Energy window (keV)	125–150	150–175
100 MBq ^{99m}Tc-TF	1.21 ± 1.5	1.01 ± 0.5
300 MBq ^{99m}Tc-TF	1.08 ± 1.4	0.98 ± 0.4

^{99m} Tc-TF ^{99m}Tc-labeled tetrofosmin

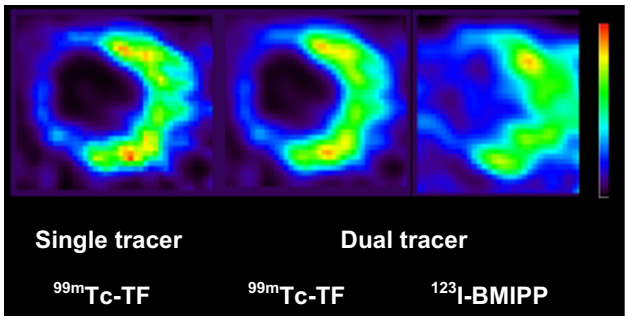

Fig. 4 SPECT images in a rat model of myocardial infarction using 300 MBq ^{99m}Tc-TF in the single tracer and 300 MBq ^{99m}Tc-TF and 100 MBq ^{123}I-BMIPP in the dual tracer. The myocardial SPECT images of ^{99m}Tc-TF in the dual tracer without SC were similar to those of ^{99m}Tc-TF in the single tracer with SC. ^{123}I-BMIPP images showed a slight mismatch with ^{99m}Tc-TF images in the posterior wall at risk of acute myocardial infarction as memory imaging

areas when SC was applied for the single tracer (Table 4). In the two syringes including high ^{99m}Tc-HMPAO dose and ^{123}I-FP-CIT, the peak of the energy spectrum of ^{99m}Tc-HMPAO was almost three times that of ^{123}I-FP-CIT (Fig. 5). Mean radioactive counts per voxel of ^{99m}Tc-HMPAO in 125–150 keV were 2.9-fold higher than that of ^{123}I-FP-CIT in 150–175 keV without SC (Table 5). Downscatter contaminations of ^{123}I-FP-CIT were approximately 1.4 % and 4.2 % of the radioactive counts for ^{99m}Tc-HMPAO in 125–150 keV with and without SC, while there was no upscatter contamination of ^{99m}Tc-HMPAO in 150–175 keV.

In the mice study, the ^{99m}Tc-HMPAO images for the dual tracer in 125–150 keV without SC were not different from those of ^{99m}Tc-HMPAO for the single tracer with SC in the first injection of ^{99m}Tc-HMPAO and second injection of ^{123}I-FP-CIT (Fig. 6). In the first injection of ^{123}I-FP-CIT and second injection of ^{99m}Tc-HMPAO, the brain images and mean radioactive counts were also not much different from those of the ^{123}I-FP-CIT single injection (Fig. 7; Table 6).

Discussion

The simultaneous acquisition of ^{99m}Tc-TF and ^{123}I-BMIPP yields myocardial blood flow and metabolism of rats under identical conditions. To detect cardiac disease more clearly, it is important for cardiac studies of rats to achieve more accurate quantification and anatomical registration between the two images of ^{99m}Tc-TF and ^{123}I-BMIPP. The quantification and anatomical registration are also crucial for brain studies of mice using ^{99m}Tc-HMPAO and ^{123}I-FP-CIT. This dual-tracer imaging accordingly reduces the experiment time and burden for research staff [6–12]. The radioactive counts and each image of simultaneously acquired ^{99m}Tc and ^{123}I were evaluated using a preclinical SPECT scanner with a CZT-based semiconductor detector. Although we can select if AC, SC and DCC are applied in the reconstruction method on this SPECT scanner, AC is not applied because AC provided low uniformity and there

Table 4 Radioactive counts per voxel of ^{99m}Tc-TF images in single tracer with SC and in dual tracer without SC for the myocardial infarction model rats

Radiotracers	Single tracer of ^{99m}Tc-TF		Dual tracer	
Region	Normal	Infarction	Normal	Infarction
Counts/voxel	289.2 ± 54.8	27.9 ± 13.5*	297.1 ± 82.5	28.3 ± 17.2*

^{99m} Tc-TF ^{99m}Tc-labeled tetrofosmin, *^{123}I-BMIPP* ^{123}I-labeled 15-(*p*-iodophenyl)-3R,S-methyl pentadecanoic acid

* $P < 0.01$ vs. normal area

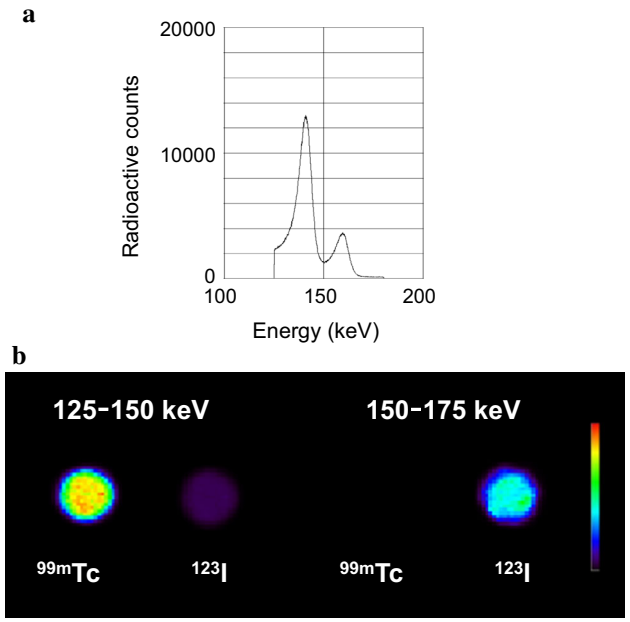

Fig. 5 Energy spectrum (**a**) and SPECT images without SC (**b**) of two 1-ml cylindrical syringes with 105 MBq ^{99m}Tc-HMPAO or 35 MBq ^{123}I-FP-CIT. Energy peak of ^{99m}Tc-HMPAO was approximately 3-fold higher than that of ^{123}I-FP-CIT. ^{99m}Tc-HMPAO image in 125–150 keV was significantly different from that of ^{123}I-FP-CIT in 150–175 keV. Downscatter contaminations of ^{123}I-FP-CIT in 125–150 keV were, respectively, approximately 1.4 and 4.2 % of the radioactive counts for ^{99m}Tc-HMPAO with and without SC

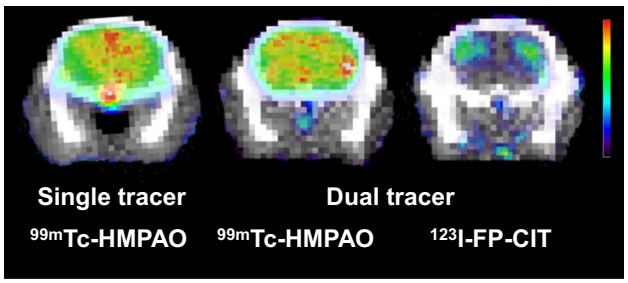

Fig. 6 Fusion images of SPECT and CT in normal mice using a single tracer of 105 MBq ^{99m}Tc-HMPAO, and dual tracers of the first injection with 105 MBq ^{99m}Tc-HMPAO and second injection with 35 MBq ^{123}I-FP-CIT. ^{99m}Tc-HMPAO images in the dual tracer without SC were similar to those of ^{99m}Tc-HMPAO in the single tracer with SC

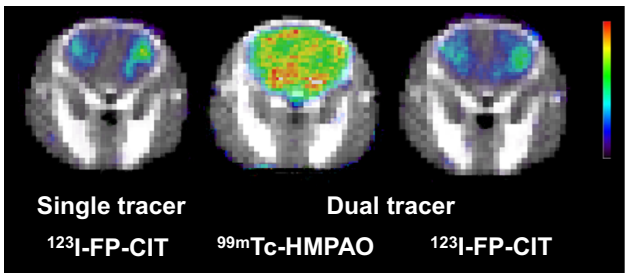

Fig. 7 Fusion images of SPECT and CT in normal mice using 35 MBq ^{123}I-FP-CIT in the single tracer, and the first injection with 105 MBq ^{99m}Tc-HMPAO and second injection with 35 MBq ^{123}I-FP-CIT in the dual tracer. ^{123}I-FP-CIT images in the dual tracer without SC were not different from those of ^{123}I-FP-CIT in the single tracer with SC

is no hard substance such as bone in the chest region including the heart and scull of the mice (0.2 mm) which is much smaller thickness than that of rats (0.5–1.0 mm) and human (about 10 mm) [21], but, DCC is always applied to improve significant SPECT images. Scatter and cross-talk effects of ^{99m}Tc and ^{123}I mainly hamper the simultaneous acquisition of dual tracers whose photon energies are close.

The relationship between SPECT radioactive counts and radioactivity of ^{99m}Tc or ^{123}I was excellent (Fig. 1). However, each radioactivity of ^{99m}Tc and ^{123}I in dual tracers could not be accurately separated and measured by dose calibrator and ex vivo autoradiography. Therefore, we used SPECT radioactive counts for evaluation of dual tracers in our study.

In the experiment with the cylindrical syringe, upscatter contamination of ^{99m}Tc-TF was not incorporated in the 150–175 keV energy window of ^{123}I-BMIPP without AC and SC (Tables 1, 2, 5). The ratio of downscatter contamination from ^{123}I-BMIPP in 125–150 keV divided by 300 MBq ^{99m}Tc-TF without SC (4.0 %) produces results similar to when divided by 100 MBq ^{99m}Tc-TF with SC in 125–150 keV (3.5 %) because downscatter contamination of ^{123}I-BMIPP exhibited fewer radioactive counts of 300 MBq ^{99m}Tc-TF.

In experiments with a rat-sized cylinder phantom (Table 3), when 300 MBq ^{99m}Tc-TF and 100 MBq ^{123}I-

Table 5 Radioactive counts per voxel in the 1-ml cylindrical syringes including high ^{99m}Tc-HMPAO dose and ^{123}I-FP-CIT

	SC–				SC+			
Energy window (keV)	125–150		150–175		125–150		150–175	
Radiotracers	^{99m}Tc-HMPAO	^{123}I-FP-CIT	^{99m}Tc-HMPAO	^{123}I-FP-CIT	^{99m}Tc-HMPAO	^{123}I-FP-CIT	^{99m}Tc-HMPAO	^{123}I-FP-CIT
Counts/voxel	407.5 ± 20.6	17.3 ± 6.1	1.1 ± 0.3	140.4 ± 8.9	368.2 ± 17.1	5.3 ± 4.6	0.5 ± 0.3	118.4 ± 6.8

SC scatter correction, *^{99m}Tc-HMPAO* ^{99m}Tc-labeled hexamethylpropyleneamine oxime, *^{123}I-FP-CIT* ^{123}I-labeled *N*-ω-fluoropropyl-2β-carbomethoxy-3β-(4-iodophenyl)nortropane

Table 6 Radioactive counts per voxel of ^{99m}Tc-HMPAO images in 125–150 keV and ^{123}I-FP-CIT images in 150–175 keV on normal mice injected single tracer with SC and dual tracer without SC

First injection	^{99m}Tc-HMPAO				^{123}I-FP-CIT	
Radiotracers	Single tracer of ^{99m}Tc-HMPAO		Dual tracer		Single tracer of ^{123}I-FP-CIT	Dual tracer
Region	WB	Striatum	WB	Striatum	Striatum	Striatum
Counts/voxel	101.8 ± 5.3	105.1 ± 8.5	106.1 ± 7.1	108.3 ± 10.2	26.9 ± 9.3	28.3 ± 8.6

^{99m}Tc-HMPAO ^{99m}Tc-labeled hexamethylpropyleneamine oxime, *^{123}I-FP-CIT* ^{123}I-labeled N-ω-fluoropropyl-2β-carbomethoxy-3β-(4-iodophenyl)nortropane, *WB* Whole brain

BMIPP were used, there was little influence from the downscatter contamination of ^{123}I-BMIPP in 125–150 keV despite SC as the radioactivity of ^{99m}Tc-TF was higher than ^{123}I-BMIPP. CZT detectors and pinhole collimators yield a narrow energy spectrum [2–6], and preclinical SPECT images are typically much less degraded by photon scattering than clinical SPECT images because of smaller body dimensions. Kao et al. has also reported that downscatter contamination of ^{123}I-ADAM was less affected by radioactive counts of ^{99m}Tc-TRODAT in dual-tracer imaging of ^{99m}Tc-TRODAT and ^{123}I-ADAM when the radioactivity of ^{99m}Tc-TRODAT was approximately 3.5-fold higher than that of ^{123}I-ADAM [12]. In addition, there was no upscatter contamination of ^{99m}Tc-TF in 150–175 keV. Therefore, each accurate radioactive count of ^{99m}Tc and ^{123}I will be provided by the narrow energy spectrum of radionuclides using a CZT detector with pinhole collimator and/or SC and DCC if the radioactivity of the injected ^{99m}Tc-TF tracer is increased. Although the simultaneous acquisition of ^{99m}Tc and ^{201}Tl has already been reported using a clinical SPECT scanner with a CZT detector, AC and DCC were not applied to measure accurate radioactive counts [6]. Especially, DCC should be applied to the simultaneous acquisition of ^{99m}Tc and ^{123}I in preclinical SPECT imaging with CZT detector. If the correction methods are unavailable, we should increase the radioactivity of ^{99m}Tc to decrease the downscatter contamination of ^{123}I.

In the rat model of myocardial infarction using 300 MBq ^{99m}Tc-TF and 100 MBq ^{123}I-BMIPP, the ^{99m}Tc-TF images in 125–150 keV without SC of the TEW method in the dual tracer were not significantly different from those of the single tracer with SC of the TEW method when DCC was applied (Fig. 3). The uptake of ^{99m}Tc-TF in the myocardial infarction significantly decreased in comparison with that in the normal area (Table 5). In ^{123}I-BMIPP images, the infarct areas showed no accumulation compared to those in ^{99m}Tc-TF images because ^{123}I-BMIPP images yielded memory imaging of the infarction area [14, 15]. In the 125–150 keV energy window, radioactive counts in dual tracers were not significantly different from those of ^{99m}Tc-TF in the single tracer in normal and infarction areas when DCC were applied (Table 5).

Since ^{123}I-FP-CIT specifically accumulates in striatum [23], we evaluated the accumulation in both ^{99m}Tc-HMPAO and ^{123}I-FP-CIT images. In *striatum* and whole brain of normal mice, the ^{99m}Tc-HMPAO images and radioactive counts in 125–150 keV for the dual tracer without SC were not different from those for the single tracer with SC in the first injection of ^{99m}Tc-HMPAO (Fig. 6; Table 6) because, in human study, accumulation of ^{99m}Tc-HMPAO maintains steady-state from early phase of 5 min to late phase of 8 h after the injection [22]. Brain images and radioactive counts of ^{123}I-FP-CIT in striatum were also similar between the single tracer of ^{123}I-FP-CIT (Fig. 7; Table 6). To decrease radioactivity of ^{99m}Tc-labeled radiotracers for dual-tracer imaging, we will develop a program for the TEW method for dual-tracer imaging in the future. In addition, we should consider the cardiac motion of rats in this study. More accurate quantification of the dual tracers may be achieved using gated SPECT.

Conclusion

Dual-tracer imaging of ^{99m}Tc- and ^{123}I-labeled radiotracers is feasible in small animal studies using a preclinical SPECT scanner with CZT detectors. Radioactivity of the injected ^{99m}Tc-labeled radiotracers should be increased as much as possible to improve quantification of ^{99m}Tc-labeled radiotracers in dual-tracer imaging if the correction methods cannot be appropriately applied. In this case, correction methods are not necessarily required for the quantification of ^{99m}Tc- and ^{123}I-labeled radiotracers when using a preclinical SPECT scanner with CZT detector.

Acknowledgments The author would like to thank Akiko Hayashi and Ryoko Komatsu, Takafumi Tsujiuchi, Masatoshi Sakashita and members of the medical staff at the Ishikawa prefectural government and Kanazawa University.

Compliance with ethical standards

Conflict of interest The authors declare that they have no conflict of interest.

Sources of funding This study was partly funded by Grants-in-Aid for Scientific Research from the Japan Society for the Promotion of Science (24601008, 24659558, 25293260 and 15K09949), the Society of Nuclear Medicine Technology, Japanese Society of Radiological Technology and Ishikawa Prefecture Commission Research.

References

1. Franc BL, Acton PD, Mari C, Hasegawa BH. Small-animal SPECT and SPECT/CT: important tools for preclinical investigation. J Nucl Med. 2008;49:1651–63.
2. Kim H, Furenlid LR, Crawford MJ, Wilson DW, Barber HB, Peterson TE, et al. SemiSPECT: a small-animal single-photon emission computed tomography (SPECT) imager based on eight cadmium zinc telluride (CZT) detector arrays. Med Phys. 2006;33:465–74.
3. Higaki Y, Kobayashi M, Uehara T, Hanaoka H, Arano Y, Kawai K. Appropriate collimators in a small animal SPECT scanner with CZT detector. Ann Nucl Med. 2013;27:271–8.
4. Matsunari I, Miyazaki Y, Kobayashi M, Nishi K, Mizutani A, Kawai K, et al. Performance evaluation of the eXplore speCZT preclinical imaging system. Ann Nucl Med. 2014;28:484–97.
5. Herzog BA, Buechel RA, Katz R, Brueckner M, Husmann L, Burger IA, et al. Nuclear myocardial perfusion imaging with a cadmium-zinc-telluride detector technique: optimized protocol for scan time reduction. J Nucl Med. 2010;51:46–51.
6. Kacperski K, Erlandsson K, Ben-Haim S, Hutton BF. Iterative deconvolution of simultaneous ^{99m}Tc and ^{201}Tl projection data measured on a CdZnTe-based cardiac SPECT scanner. Phys Med Biol. 2010;56:1397–414.
7. El Fakhri G, Maksud P, Kijewski MF, Habert MO, Todd-Pokropek A, Aurengo A, et al. Scatter and cross-talk corrections in simultaneous Tc-99 m/I-123 brain SPECT using constrained factor analysis and artificial neural networks. IEEE Trans Nucl Sci. 2000;47:1573–80.
8. El Fakhri G, Moore SC, Maksud P, Aurengo A, Kijewski MF. Absolute activity quantitation in simultaneous ^{123}I/^{99m}Tc brain SPECT. J Nucl Med. 2001;42:300–8.
9. Ouyang J, Zhu X, Trott CM, El Fakhri G. Quantitative simultaneous ^{99m}Tc/^{123}I cardiac SPECT using MC-JOSEM. Med Phys. 2009;36:602–11.
10. Du Y, Tsui BM, Frey FC. Model-based crosstalk compensation for simultaneous ^{99m}Tc/^{123}I dual-isotope brain SPECT imaging. Med Phys. 2007;34:3530–43.
11. Du Y, Frey EC. Quantitative evaluation of simultaneous reconstruction with model-based crosstalk compensation for 99mTc/123I dual-isotope simultaneous acquisition brain SPECT. Med Phys. 2009;36:2021–33.
12. Kao PF, Way SP, Yang AS. Simultaneous ^{99m}Tc and ^{123}I dual-isotope brain striatal phantom single photon emission computed tomography: validation of ^{99m}Tc-TRODAT1 and ^{123}I-IBZM simultaneous dopamine system brain imaging. Kaohsiung J Med Sci. 2009;25:601–7.
13. Higley B, Smith FW, Smith T, Gemmell HG, Das Gupta P, Gvozdanovic DV, et al. Technetium-99m-1,2-bis [bis(2-ethoxyethyl) phosphino]ethane: human biodistribution, dosimetry and safety of a new myocardial perfusion imaging agent. J Nucl Med. 1993;34:30–8.
14. Tateno M, Tamaki N, Yukihiro M, Kudoh T, Hattori N, Tadamura E, et al. Assessment of fatty acid uptake in ischemic heart disease without myocardial infarction. J Nucl Med. 1996;37:1981–5.
15. Mochizuki T, Murase K, Higashino H, Miyagawa M, Sugawara Y, Kikuchi T, et al. Ischemic "memory image" in acute myocardial infarction of ^{123}I-BMIPP after reperfusion therapy: a comparison with ^{99m}Tc-pyrophosphate and ^{201}Tl dual-isotope SPECT. Ann Nucl Med. 2002;16:563–8.
16. Reutter BW, Huesman RH, Brennan KM, Boutchko R, Hanrahan SM, Gullberg GT. Longitudinal evaluation of fatty acid metabolism in normal and spontaneously hypertensive rat hearts with dynamic microSPECT imaging. Internal J Mol Imag. 2011;. doi:10.1155/2011/893129.
17. Walrand S, Jamar F, de Jong M, Pauwels S. Evaluation of novel whole-body high-resolution rodent SPECT (Linoview) based on direct acquisition of linogram projections. J Nucl Med. 2005;46:1872–80.
18. Zheng GL, Gagnon D. CdZnTe strip detector SPECT imaging with a slit collimator. Phys Med Biol. 2004;49:2257–71.
19. Strydhorst JH, Ruddy TD, Wells RG. Effects of CT-based attenuation correction of rat microSPECT images on relative myocardial perfusion and quantitative tracer uptake. Med Phys. 2015;42:1818–24.
20. Ichihara T, Ogawa K, Motomura N, Kubo A, Hashimoto S. Compton scatter compensation using the triple-energy window method for single- and dual-isotope SPECT. J Nucl Med. 1993;34:2216–21.
21. O'Reily MA, Muller A, Nynynen K. Ultrasound insertion loss of rat parietal bone appears to be proportional to animal mass at submegahertz frequencies. Ultrasound Med Biol. 2011;37:1930–7.
22. Sharp PF, Smith FW, Gemmell HG, Lyall D, Evans NT, Gvozdanovic D, Davidson J, Tyrrell DA, Pickett RD, Neirinckx RD. Technetium-99m HM-PAO stereoisomers as potential agents for imaging regional cerebral blood flow: human volunteer studies. J Nucl Med. 1986;27:171–7.
23. Miia Pitkonen, Eero Hippeläinen, Mari Raki, Jaan-Olle Andressoo, Arto Urtti, Pekka T Männistö, Sauli Savolainen, Mart Saarma, Kim Bergström. Advanced brain dopamine transporter imaging in mice using small-animal SPECT/CT. EJNMMI Res. 2012; 2: 55. Published online 2012 September 29. doi: 10.1186/2191- 219X-2-55.